

A Revised Characterization of the WFPC2 CTE Loss

Andrew E. Dolphin

Raytheon Company, Tucson, AZ 85756

adolphin@raytheon.com

ABSTRACT

Charge-transfer loss on the Wide Field Planetary Camera 2 (WFPC2) onboard the Hubble Space Telescope is a primary source of uncertainty in stellar photometry obtained with this camera. This effect, discovered shortly after the camera was installed, has grown over time and can dim stars by several tenths of a magnitude (or even more, in particularly bad cases). The impact of CTE loss on WFPC2 stellar photometry was characterized by several studies between 1998 and 2000, but has received diminished attention since ACS became HST's primary imager. After the failure of ACS in January 2007, WFPC2 once again became the primary imaging instrument onboard HST, restoring the importance of ensuring accurate CTE corrections.

This paper re-examines the CTE loss of WFPC2, with three significant changes over previous studies. First, the present study considers calibration data obtained through 2007, thus increasing the confidence in the reliability of the CTE corrections when applied to recent observations. Second, the change in CTE loss during readout is accounted for analytically. Finally, a reanalysis of the CTE dependencies on counts, background, and observation date was made. The resulting correction is significantly more accurate than that provided in the WFPC2 Instrument Handbook (Dolphin 2002 and updates through 2004), resulting in photometry that can be enhanced by over 5% in certain circumstances.

Subject headings: data analysis and techniques

1. Introduction

Shortly after its installation onboard the Hubble Space Telescope in 1994, the Wide Field Planetary Camera 2 (WFPC2) was observed to suffer from charge-transfer loss, a phenomenon in which charge is removed from a star's image during CCD readout (Holtzman et al.

1995a). The effect of this inefficiency is to reduce the star’s apparent brightness, especially those with large Y (parallel-read direction) values on the CCDs (and, to a lesser extent, those with large X values). An initial solution to this was to cool the camera from -76°C to -88°C to reduce the magnitude of the effect, and to apply a correction that scaled from linearly from zero for stars with $Y = 0$ to a maximum of 0.04 magnitudes for stars with $Y = 800$. Holtzman et al. (1995a) also noted that the CTE loss appeared to be a function of background level, and recommended no CTE correction for images with backgrounds over ~ 250 electrons.

This dependency of CTE on background, as well as dependencies on star brightness and observation date, were quantified by Whitmore & Heyer (1997) and updated by Whitmore (1998), who found that the CTE loss in the Y direction could be corrected by an equation with the form

$$\text{CTS}_{\text{corr}} = \text{CTS} \times [1 + f_1(\text{CTS}) \times f_2(\text{BG}) \times f_3(\text{DATE}) \times Y],$$

where CTS is the star’s brightness on the read-out image; BG is the background level; DATE is the date of observation; and f_1 , f_2 , and f_3 are used to denote functions. (Whitmore et al. used power law functions for both f_1 and f_2 , and a linear function for f_3 .)

In addition to reports from the WFPC2 team, characterizations of CTE loss in the refereed literature were made by Stetson (1998), Whitmore, Heyer, & Casertano (1999), Saha, Labhardt, & Prosser (2000), and Dolphin (2000a, hereafter D00). Differences in the assumed functional form of the solution and in the photometry techniques resulted in somewhat different correction prescriptions. However, D00 found reasonable agreement between the corrected magnitudes being produced by each of the four.

Since that time, there have been several significant issues requiring continued examination of the effects of CTE loss on WFPC2 stellar photometry. Most notable, given the time dependence of CTE loss, is the question of the applicability of published CTE corrections to data being currently obtained. Especially given the increased utilization of WFPC2 during cycles 15 and 16, reinvestigation of CTE issues can greatly increase confidence in the photometry being generated.

Other concerns are related to the functional form of the CTE corrections themselves, due to limited ranges of star brightness and background level of the calibration observations. Whitmore & Heyer (2002) examined the validity of existing CTE correction equations on stars significantly fainter than had been previously examined. While it was encouraging that the D00 corrections were valid when applied to stars as faint as 100 electrons (thus, the corrections are accurate for the vast majority of data used by WFPC2 science programs), for yet fainter stars these corrections appeared to overestimate the CTE loss by ~ 0.2

magnitudes.

Likewise, there is the open question of the applicability of existing CTE corrections to higher background levels (specifically, those typical of deep science exposures). Early work on WFPC2 CTE loss relied primarily on data taken with very low background levels (mostly less than 10 electrons), which required assumptions to be made regarding the effect of background level on CTE loss. However, since 2000, WFPC2 calibration programs have increasingly made use of the camera’s preflash capability, in which the CCDs are pre-exposed with a flat-field lamp before the actual observation. (A preflashed short exposure with bright stars is frequently used to simulate the CTE loss seen in much longer observations of fainter stars.) These data permit a significantly more accurate measurement of the effects of CTE loss on higher-background data.

This paper re-evaluates the CTE corrections in light of these three concerns, using calibration data obtained through August 2007. Section 2 describes the data used in this study, section 3 contains preliminary analysis of the functional forms required for accurate CTE corrections, section 4 contains the CTE corrections themselves, and section 5 examines effects of the new corrections.

2. Observations

As with D00 and Dolphin (2002, hereafter D02), the data used for this study were observations of the WFPC2 calibration field in ω Cen. (To select the data, an HST archive search was made within 1.5 arcmin of $\alpha = 13^h25^m37^s$ and $\delta = -47^\circ35'58''$.) Only cold-camera (-88°C) images were considered. A total of 1184 data sets were photometered: 142 in F439W, 300 in F555W, 92 in F675W, 573 in F814W, and 77 in the other *BVRI* filters, with the most recent observations taken in August 2007.

The data were reduced using HSTphot¹ (Dolphin 2000b), following the recommended reduction recipe in the HSTphot manual except as follows. First, in the initial sky solution, the “abbreviated” mode of `getsky` was used. Second, `hstphot` was executed with an iterated sky solution during the photometry process (option 512), CTE corrections turned off and photometry calibrated according to Holtzman et al. (1995b) (option 32), and aperture photometry (option 1). The lone option of note is the use of aperture photometry, which increases photometric uncertainties but is more robust (PSF-fitting photometry can induce artificial nonlinearities if the PSF is not *exactly* correct) and thus better suited for this

¹<http://purcell.as.arizona.edu/hstphot/>

analysis.

To avoid complications resulting from the WF4 anomaly (Biretta & Gonzaga 2005), all WF4 observations from SM3B (March 2002) onwards were omitted from this study.

For this analysis, the WFPC2 data were compared against ground-based *BVRI* calibration data of Walker (1994). To facilitate this comparison, the *BVRI* magnitudes were transformed to WFPC2 instrumental magnitudes using the color terms of Holtzman et al. (1995b).

After excluding data that failed to meet data quality requirements, 55286 stellar measurements were matched to the ground-based standard data. Statistics of the brightness, background, and observation date distributions are presented in Table 1.

3. Analysis

Prior to attempting a generic solution for CTE loss as a function of star brightness, background level, and date of observation; it is worthwhile to examine each of these variables in isolation. In order to do this, the data have been selected to constrain two of these variables to limited ranges, allowing an examination of the third. For example, to analyze CTE loss dependence on date of observation, a limited range of star brightness and background level was chosen. The data were then divided into groups based on observation date, and each group of data was fit as follows:

$$m_{WFPC2} - m_{ground} = a + b\frac{x}{800} + c\frac{y}{800}, \quad (1)$$

where the left hand side is the magnitude difference between the WFPC2 and the ground-based standard data. The fit coefficients a , b , and c give position-independent, XCTE, and YCTE terms respectively, and are examined in the subsequent sections.

3.1. Position-independent Errors

In addition to CTE loss, there have also been many concerns regarding photometric errors that are not position-dependent, such as zero point offsets and the long-vs-short anomaly (Casertano & Mutchler 1998). Variations in the intercept of the fit from Equation 1 vs. star brightness and vs. background level are shown in Figure 1. (Note that position-independent errors vs. observation date are merely time variations in the WFPC2 sensitivity, and are tracked extensively by the instrument team and thus not addressed in this study.)

From the figure, one sees that no significant trends in the data are present. Quantitatively, the data permit one to place a 1σ upper limit of 0.025 magnitudes per dex of either star brightness or background level over the ranges of each shown in the figure.

It should be noted that this finding not only dispels the presence of a large long-vs-short anomaly, but also provides additional confidence regarding the validity of the comparison between the ground-based standard field and the WFPC2 observations. Specifically, were any error as a function of color present (which would masquerade as an error as a function of magnitude, given the nature of this field), it would have been seen in Figure 1. As no such error was observed, the confidence in the validity of this comparison is enhanced.

What is measured, however, is a mean zero point offset relative to the Holtzman et al. (1995b) calibrations. Averaging the three plots of F555W data, the mean residual (WFPC2 minus ground) is ~ -0.06 magnitudes, while the mean for the three plots of F814W data is ~ -0.03 magnitudes. Thus, a correction to the zero points will be needed in order to adequately match the WFPC2 observations to the standard data.

3.2. XCTE

While YCTE loss is easy to measure by eye and has grown significantly over the years, XCTE loss has always had a small (though measurable) effect on stellar photometry on WFPC2. Figure 2 shows XCTE loss as a function of star brightness and of background level.

As can be seen from the figure, dependencies of XCTE on the independent variables is not obvious. (This is also true of variations in XCTE as a function of observation date, not shown in Figure 2.) Thus, determination of XCTE dependencies will be left for statistical methods in Section 4.

3.3. YCTE vs. Date

Figure 3 shows YCTE loss as a function of date of observation. To provide an indication of how this function is affected by star brightness and background levels, three sets of data are shown: faint stars on low background (panel a), bright stars on low background (panel b), and bright stars on higher background (panel c). While these samples do not represent the extremes of the data shown in Table 1, these are the largest baselines containing sufficient numbers of stars to see clear trends.

An examination of panels (a) and (b) of Figure 3 indicates that, despite nearly a factor of two difference in YCTE loss between faint and bright stars in recent observations (both on low backgrounds), both sets of data show similar YCTE losses during the earliest observations. Specifically, quadratic fits to the curves give YCTE losses of 0.054 ± 0.005 magnitudes for faint stars (panel a) and 0.058 ± 0.004 magnitudes for bright stars (panel b) for an observation date of 1994.3 (20 April 2004). This indicates that the two curves are not merely scaled versions of each other. It should also be noted that the same dependence on observation date is seen in both curves, such that panels (a) and (b) both fall onto the curve:

$$\Delta m = 0.056 + (\Delta \text{yr} - 0.027\Delta \text{yr}^2) \times f(\text{CTS}),$$

where Δyr is the year minus 1994.3.

The data for higher background levels are not nearly as complete, due to few high-background observations of this field made prior to mid-1998. The data in Figure 3c are consistent with both the same intercept at 1994.3, as well as a lower one. In other words, determination of whether the functional form should be

$$\Delta \text{mag} = 0.056 + (\Delta \text{yr} - 0.027\Delta \text{yr}^2) \times f(\text{CTS}) \times f(\text{BG}) \quad (2)$$

or

$$\Delta \text{mag} = [0.056 + (\Delta \text{yr} - 0.027\Delta \text{yr}^2) \times f(\text{CTS})] \times f(\text{BG}) \quad (3)$$

must wait until the analysis of the full data set is made. It should be noted that the calibration data used by Holtzman et al. (1995a) showed a strong background dependence of YCTE loss for observations obtained in 1994: 0.04 magnitudes of loss (at $Y = 800$) for measurements with background levels $\lesssim 20 - 30$ electrons, 0.02 magnitudes for background levels $\sim 30 - \sim 250$ electrons, and zero for higher background levels. Thus, the functional form in Equation 3 is to be preferred unless the present data set demonstrate otherwise.

3.4. YCTE vs. Star Brightness

Figure 4 shows YCTE loss as a function of star brightness, with data selected to show recent observations with low background (panel a), old observations with low background (panel b), and intermediate-age observations with higher background (panel c).

The trend from panels (a) and (b) is that the slope of the curve decreases as star brightness increases, which suggests the use of an exponential for the CTE variation as a function of brightness.

Considering only points for which YCTE loss is less than 0.5 magnitudes (see Section 3.6 for a discussion of the treatment of large CTE losses) and using the results of the previous section, both curves can be fitted with the formula:

$$\Delta m = 0.056 + 1.2(\Delta \text{yr} - 0.027\Delta \text{yr}^2) \times e^{-0.43 \ln(\text{CTS})}.$$

Effects of background on the YCTE loss vs. counts will be discussed in Section 3.5.

3.5. YCTE vs. Background

The final independent variable considered in this analysis is the background level. Figure 5 shows CTE loss as a function of background, for faint stars observed in roughly 2001 (panel a), faint stars observed in 1995 (panel b), and bright stars observed in 2001 (panel c). As with D00 and D02, a “softened” background was used, which equals $\sqrt{1 + \text{BG}^2}$ electrons (and is 1 if the measured background level is negative). This softened background compresses the lowest background levels, making it easier to find a functional form for fitting CTE loss vs. background.

The YCTE plots in Figure 5 do not show the curvature characteristic of an exponential decay, suggesting that a line be used instead to fit the YCTE dependence on background. Another significant feature of the background dependence, although the data used to generate Figure 5 contain insufficient stars to make this evident, is that the slope of the relation is shallower for bright stars than it is for faint stars. Thus, the function used to fit the background dependence is

$$f(\text{BG}) = \max[(1 - c_1 \ln \text{BG} + c_2(\ln \text{BG} - c_3) \ln \text{CTS}), c_4].$$

3.6. Charge Loss During Readout

When CTE loss removes a significant fraction of a star’s overall brightness, one must take into account the fact that the CTE loss rate itself changes as the star is read out. Using the customary terminology of losses as fractions of star brightness lost (as opposed to number of electrons lost) per pixel read out, the CTE loss rate will increase during readout since the loss rate increases as the star becomes fainter.

The exact relation can be determined fairly simply. Let the charge lost per pixel transferred be expressed as a differential equation with the form

$$\frac{dx}{dy} = -a - be^{-cx}, \tag{4}$$

where x is the natural logarithm of the star’s brightness; and a , b , and c are constants (or functions of background level and observation date, which are both constant during the readout process). If the star’s brightness were to remain essentially unchanged during readout (i.e., CTE loss is a small fraction of the star’s brightness), the loss per pixel traversed would be constant as well. This would result in a magnitude loss Δm of

$$\Delta m = 1.086Y(a + be^{-cx}), \quad (5)$$

where Y is the star’s Y position on the chip. The multiplier of 1.086 converts from differences in natural logarithm to differences in magnitude. Note that this general form is seen in the literature correction equations (Whitmore 1998; Stetson 1998; Whitmore et al. 1999; D00).

However, for very faint stars, the amount of CTE loss can be significant, and thus one cannot safely assume that CTE loss remains constant during readout. Solving Equation 4, the magnitude loss is given by

$$\Delta m = \frac{1.086}{c} \ln \left[e^{acy} \left(1 + \frac{b}{a} e^{-cx} \right) - \frac{b}{a} e^{-cx} \right], \quad (6)$$

where x is the natural logarithm of the measured counts (after any loss due to readout). Note that, if $acy \ll 1$, this equation simplifies to Equation 5. For larger values of acy , this produces a smaller CTE correction than Equation 5.

It should be noted that a CTE correction derived from data including extremely faint stars should implicitly include this effect, as the lower CTE loss would have been in the measurements and thus in the correction. However, most CTE corrections (such as that presented in this paper) are based only on brighter stars, due to the practical difficulty in obtaining sufficiently accurate photometry of extremely faint stars. Thus, the brightness dependence in the CTE corrections is measured using brighter stars for which Equations 5 and 6 produce the same result. Assuming that the brightness dependence is correct (given the extrapolation involved, it may not be), the form of the correction from Equation 6 will be required to correctly model CTE loss of faint stars.

This effect is illustrated in Figure 6. To produce this figure, observations of the ω Cen standard field, taken on 17 August 2000 as part of calibration program GO-8447, were analyzed. The observations consisted of one 100-second F814W exposure and two 14-second F814W exposures (as well as other exposures using different filters and preflashes) at each of two pointings. For each pointing, HSTphot was used to obtain photometry for the 100-second exposure as well as the average of the 14-second exposures. Figure 6 shows ratios of the 14-second to 100-second count levels after applying CTE corrections of the forms in Equations 5 and 6. The horizontal line in the figure is at a ratio of 0.14, which is what would be expected in the absence of CTE loss.

As is clear from the figure, the form of the CTE correction that accounts for CTE loss during readout significantly reduces systematic errors in the correction. This also bolsters confidence that the CTE corrections presented in the next section are valid for stars significantly fainter than those used for to compute the corrections themselves.

4. CTE Corrections

Guided by the analysis from the previous section, a solution was made for zero points and CTE corrections. Several fits were made, with variations on the form of the CTE correction. The form that produced the best fit to the data was

$$\frac{dm}{dx} = c_1 \times \text{BG}^{-c_2} \times (1 + c_3 \text{DATE}) \quad (7)$$

and

$$\begin{aligned} \frac{dm}{dy} = & \{c_4 + c_5[(\text{DATE} - c_6) - c_7(\text{DATE} - c_6)^2] \text{CTS}^{-c_8}\} \\ & \times \max[(1 - c_9 \ln \text{BG} + c_{10} \ln \text{BG} \ln \text{CTS} + c_{11} \ln \text{CTS}), c_{12}], \end{aligned} \quad (8)$$

where BG is the background level, CTS is the star’s brightness, DATE is the observation date, and the left-hand sides are the magnitude loss per pixel read out in the x and y directions. Note that this form is not exactly that from Equation 4, as the star’s brightness appears twice. However, as long as c_{10} is sufficiently small that changes to the star’s brightness during readout do not significantly affect the BG term, the solution in Equation 6 can be used.

After obtaining the best fit to the CTE correction parameters (and zero point differences), the “standard” photometry was redetermined from the corrected WFPC2 data. The rationale is that 1184 WFPC2 data sets ought to produce photometry that is superior to that of the original calibration data. In addition, while the results from section 3.1 indicate that issues with the ground-based photometry (such as errors in color corrections) do not generate any significant error in the WFPC2 vs. ground comparison, this will eliminate any chance that even a small error in the ground-based data would affect the measured CTE corrections.

The only negative aspect to this use of WFPC2-measured standard data to measure WFPC2 CTE losses is that the form of the CTE solution will implicitly become part of the standard photometry used to derive the CTE solution – a sort of circular logic. However, Figure 7 shows the original and updated CMDs, and it is clear that a huge improvement in the standard photometry was obtained by making this improvement without introducing biases. Were one to repeat this process – measure the CTE losses from the new standard

photometry, determine yet newer standard photometry, redetermine the CTE losses, and so on – the standard photometry would change by at most 1%, as shown in Panel (d) of Figure 7. Thus, the CTE solution recommended here is the one with a single iteration on the standard magnitudes. Naturally, the suggested zero points are based on the original ground-based standards.

To verify that the recommended solution is truly the best fit, alternative solutions made the following modifications to the functional form:

- adding a brightness dependence to the XCTE correction. This produced a null result (i.e., the dependency was zero to within the uncertainties).
- using an exponential function of background (instead of a power law) in the XCTE correction. This produced a small degradation in the quality of the fit. Due to the small size of the XCTE correction, this is of minimal significance.
- adopting a background dependence of the form in Equation 2 (instead of that in Equation 3). Due to the lack of high-background observations of this field early in WFPC2’s lifetime, there was no statistical difference between the quality of the fits. It was therefore decided to adopt the form from Equation 3, whose solution for early observations is in strong agreement with the CTE characterization of Holtzman et al. (1995a).
- moving the count dependence also outside the brackets in Equation 3. This was is the most common form in literature CTE corrections, including D00 and D02. This produced a significantly worse fit, and can be ruled out.
- using a power law for the YCTE background dependence. This was also used in most literature corrections, including D00 and D02. This also produced a significantly worse fit, and can be ruled out.

The recipe for correcting CTE loss is as follows. Given a star brightness CTS , background level BG (both in electrons), observation date $DATE$ (in MJD), and star position on the image X and Y , the following sequence of calculations will provide the $XCTE$ and $YCTE$ losses, both in magnitudes.

$$\text{lb}g = \frac{1}{2} \ln(BG^2 + 1) - 1 \tag{9}$$

$$\text{yr} = \frac{DATE - 49461.9}{365.25} \tag{10}$$

$$XCTE = 0.0077e^{-0.50\text{lb}g}(1 + 0.10\text{yr})\frac{X}{800} \tag{11}$$

$$\text{lct} = \ln(\text{CTS}) + 0.921XCTE - 7 \quad (12)$$

$$c = 0.958(\text{yr} - 0.0255\text{yr}^2)e^{-0.450\text{lct}} \quad (13)$$

$$YCTE = 2.41 \ln[(1 + c)e^{0.02239 \max(1.0 - 0.201\text{lbg} + 0.039\text{lbg}[\text{lct} + 0.002\text{lct}, 0.15])(Y/800)} - c] \quad (14)$$

Note that the offsets of 1 for lbg and 7 for lct were put in place for numerical stability, and do not affect the solution itself.

The zero points of the four primary filters (F439W, F555W, F675W, and F814W) were measured independently for each chip and gain setting (thus, a total of eight zero points per filter). For other filters, the relatively small number of available data sets required that their zero points be characterized with a single offset relative to the zero point of the nearest primary filter.

Zero points for both gain settings are provided in Tables 2 and 3. Instrumental magnitudes can be computed using

$$m_{WFPC2} = -2.5 \log(\text{counts/sec}) + ZP - XCTE - YCTE, \quad (15)$$

where the counts/second rate is measured within an aperture whose diameter is one arcsecond.

The *BVRI* transformations of Holtzman et al. (1995b) have also been modified to account for the new zero points, and are provided in Table 4. (Note that the color terms have been adopted without modifications, and are reprinted here for convenience.) Standard *BVRI* magnitudes can be computed with the following equation:

$$SMAG = -2.5 \log(\text{counts/sec}) + ZP + T1 \times SCOL + T2 \times SCOL^2 - XCTE - YCTE. \quad (16)$$

For instances in which a single set of parameters does not describe the relation sufficiently well for all colors, the Cmin and Cmax columns of Table 4 show the color range for which the table row is valid. Again, the count rate is measured within an aperture whose diameter is one arcsecond.

4.1. Verification

To verify the accuracy to which the data are being corrected, Figures 8, 9, and 10 show the YCTE residuals after zero point and CTE corrections have been applied. These plots are generated similarly to Figures 3–5, although larger data selections have been used.

With the possible exceptions of the background dependence for early observations (Figure 9d), no significant trends remain in the data. It should also be noted that the upward

trend in Figure 9d is based on very little data; only 544 star measurements (of the 22603 used for the data in this panel) had background levels of 20 or more electrons.

5. Consequences of the New Formulae

Comparing the CTE corrections from this work with those of D02, the CTE corrections agree to within 0.02 magnitudes for over 80% of the star measurements. Stars for which the current corrections are more than 0.02 magnitudes larger fall primarily into two categories: bright stars on a bright background, and dim stars (brightnesses of a few hundred electrons) on backgrounds of a few electrons. Not surprisingly, stars for which the current corrections are more than 0.02 magnitudes smaller also fall into two categories: bright stars on a low background (one electron or less), and dim stars on bright backgrounds.

The reason for the difference is the term allowing the background correction slope to change as a function of star brightness, which was not present in the D02 CTE equation. To verify that the new corrections indeed fit the data better, Figure 11 shows the residuals for both sets of CTE corrections, plotted versus the difference between the CTE corrections. The relation between CTE difference and residual is clear in Figure 11a, and in fact has a slope of one. Using the corrections from this paper, no trend of residual as a function of CTE difference exists (Figure 11b).

Given that typical science exposures have background levels higher than is typical in calibration exposures, this result can have a significant on the analysis of WFPC2 data.

6. Summary

The study presented here revisits the topic of WFPC2 charge transfer inefficiency, building on results of previous work (D00, D02). This examination is overdue, as the existing CTE characterizations are several years old and thus application to current WFPC2 observations requires significant extrapolation of the calibration data to the current epoch.

In addition to incorporation of more recent calibration data, several other enhancements were made over the previous work. Most significantly, it was seen that the effects of star brightness and background level cannot be treated independently. Making this assumption gave reasonable CTE corrections for stars whose brightness or background level was typical of calibration data. However, for higher background levels, the older CTE corrections will undercorrect bright stars and overcorrect faint stars. For bright stars, the resulting systematic error can significantly exceed the random error from photon noise.

Other significant changes from the earlier work include accounting for the change in CTE loss during readout, an improved functional form for the background dependence, and a count dependence that begins at zero at the beginning of the WFPC2 mission.

As additional calibration data become available, updated WFPC2 calibration data will be made available on the author's website².

Based on observations made with the NASA/ESA Hubble Space Telescope, obtained from the data archive at the Space Telescope Science Institute. Support for this work was provided by NASA through grant number AR-11244 from the Space Telescope Science Institute, which is operated by AURA, Inc., under NASA contract NAS 5-26555.

Facilities: HST (WFPC2).

REFERENCES

- Biretta, J. & Gonzaga, S. 2005, Instrument Science Report WFPC2 05-02
- Casertano, S. & Mutchler, M. 1998, Instrument Science Report WFPC2 98-02
- Dolphin, A. E. 2000a, PASP, 112, 1397
- Dolphin, A. E. 2000b, PASP, 112, 1383
- Dolphin, A. E. 2002, 2002 HST Calibration Workshop, ed. S. Arribas, A. Koekemoer, & B. Whitmore, 301
- Holtzman, J. A. et al. 1995, PASP, 107, 156
- Holtzman, J. A. et al. 1995, PASP, 107, 1065
- Saha, A., Labhardt, L., & Prosser, C. 2000, PASP, 112, 163
- Stetson, P. B. 1998, PASP, 110, 1448
- Walker, A. R. 1994, PASP, 106, 828
- Whitmore, B. & Heyer, I. 1997, Instrument Science Report WFPC2 97-08
- Whitmore, B. 1998, Technical Instrument Report WFPC2 98-01

²http://purcell.as.arizona.edu/wfpc2_calib/

Whitmore, B. & Heyer, I. 1997, Instrument Science Report WFPC2 02-03

Whitmore, B., Heyer, I., & Casertano, S. 1999, PASP, 111, 1559

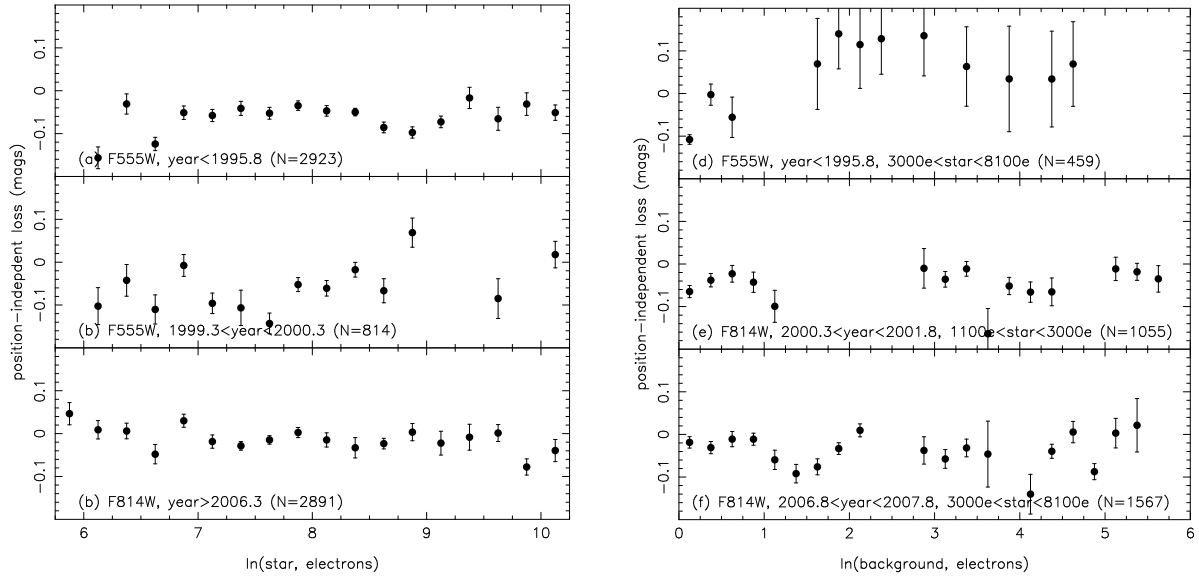


Fig. 1.— Position-independent photometry errors, shown vs. star brightness (left) and background level (right). The data selections are shown in each panel. Note that, aside from offsets (zero point errors), no clear trends are visible.

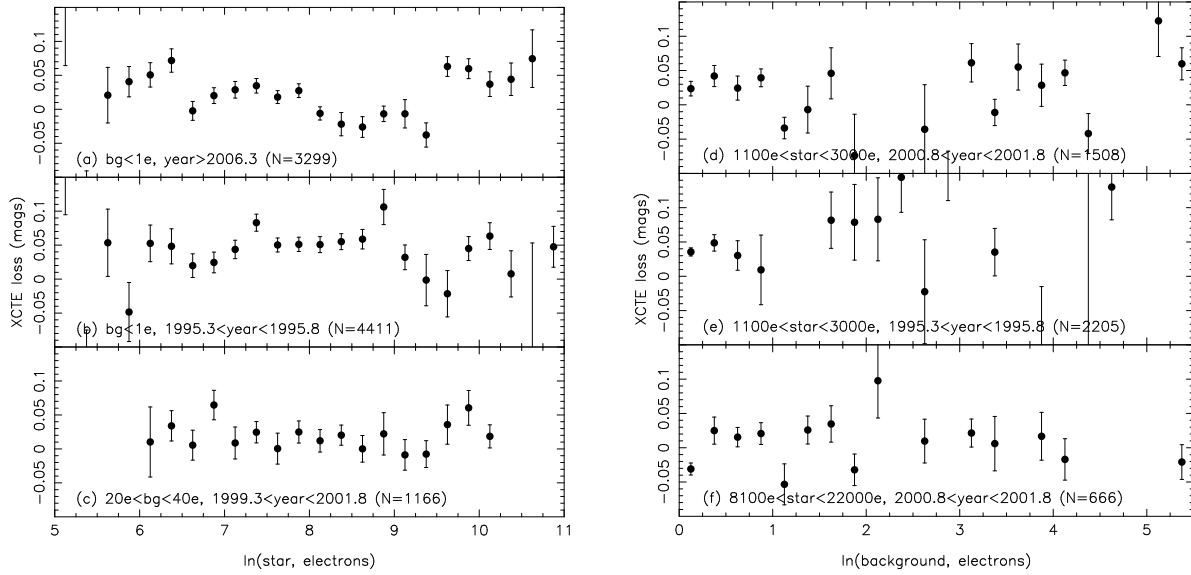


Fig. 2.— XCTE losses, as a function of star brightness (left) and background level (right). The data selections are shown in each panel. Due to the small size of XCTE losses, trends are not obvious from the figure.

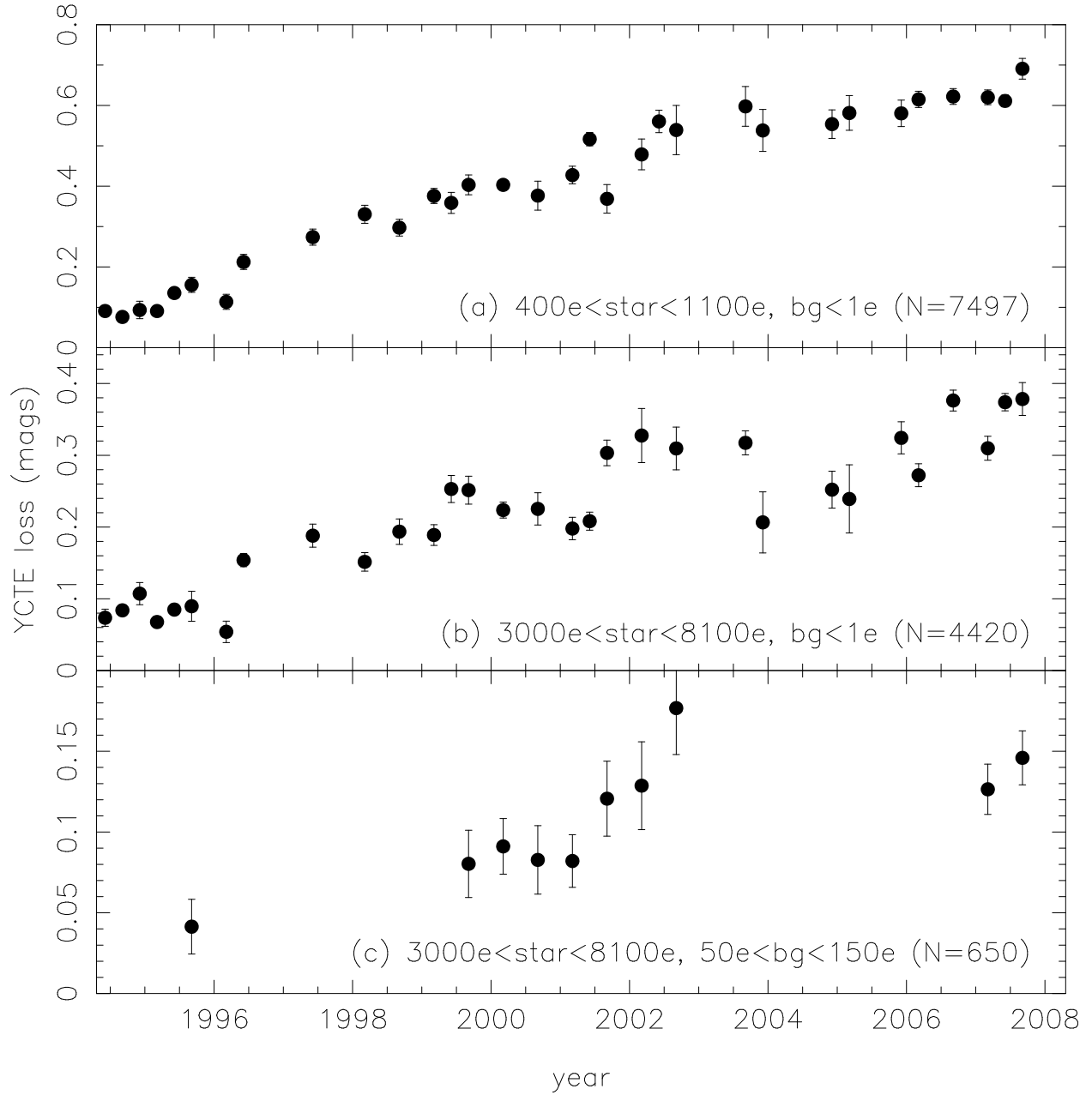


Fig. 3.— YCTE losses, as a function of observation date. Cuts in star brightness and background level are shown in the respective panels.

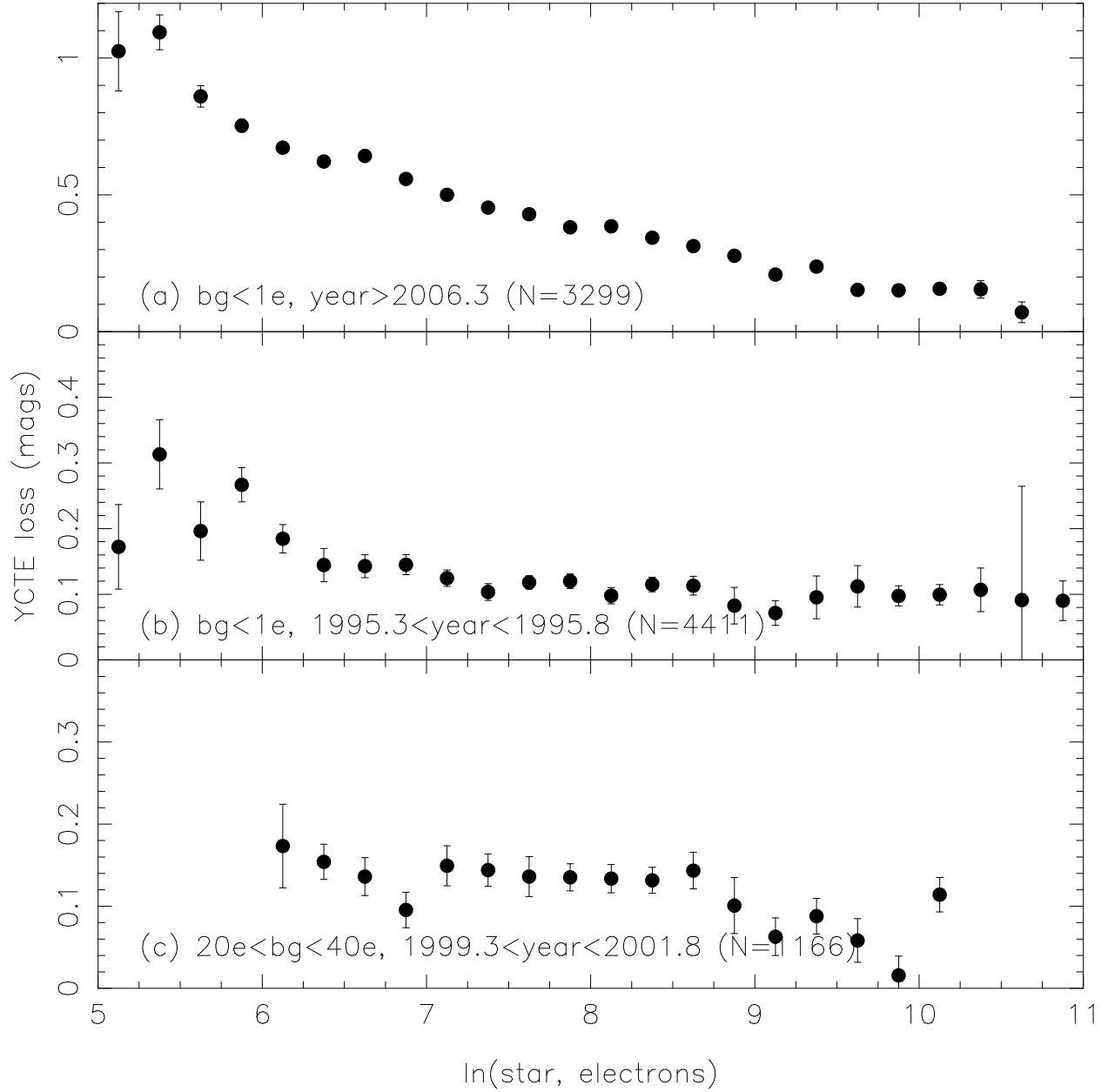


Fig. 4.— YCTE losses, as a function of star brightness. Cuts in background level and observation date are shown in the respective panels.

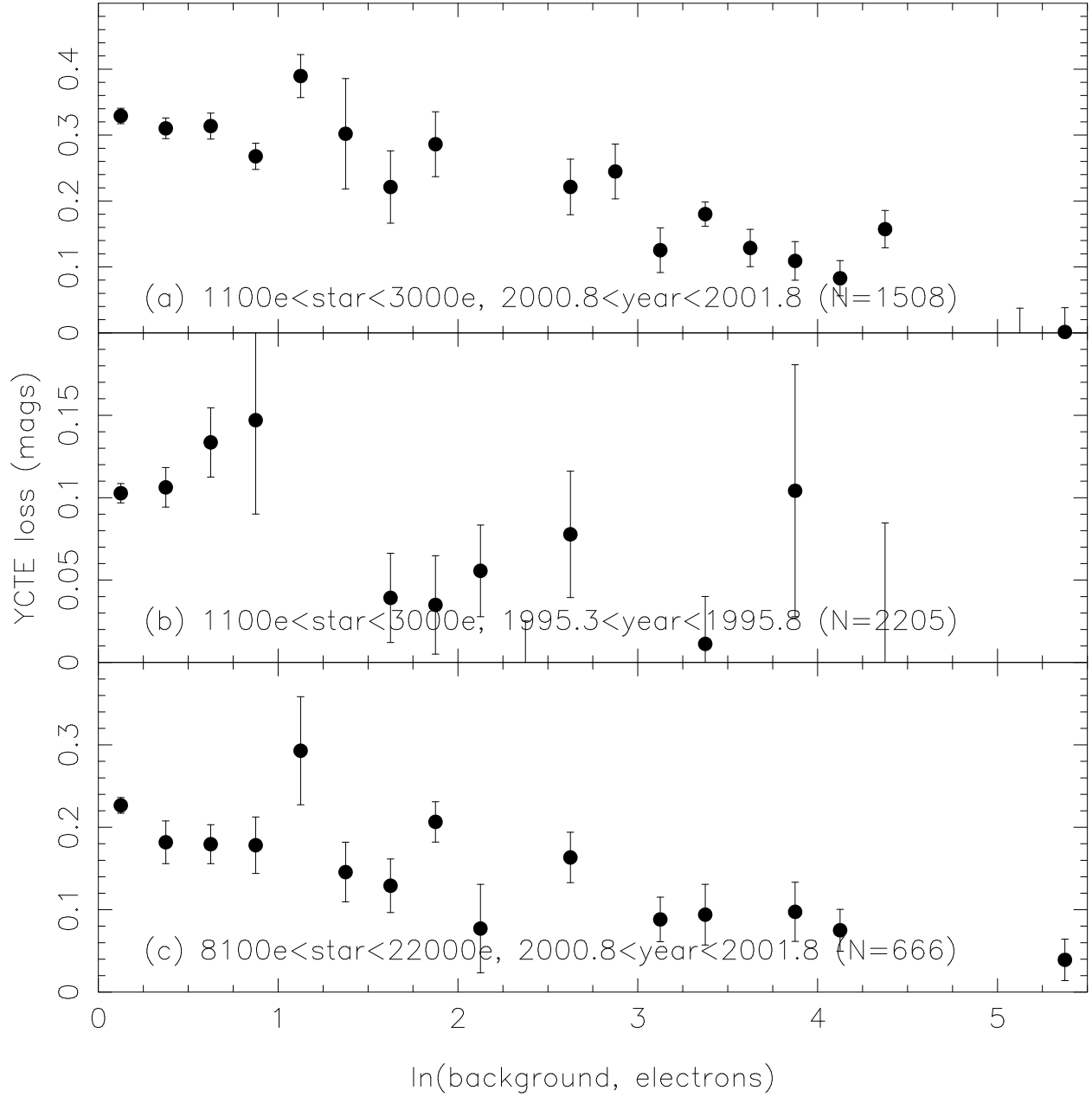


Fig. 5.— YCTE losses, as a function of background level. Cuts in star brightness and observation date are shown in the respective panels.

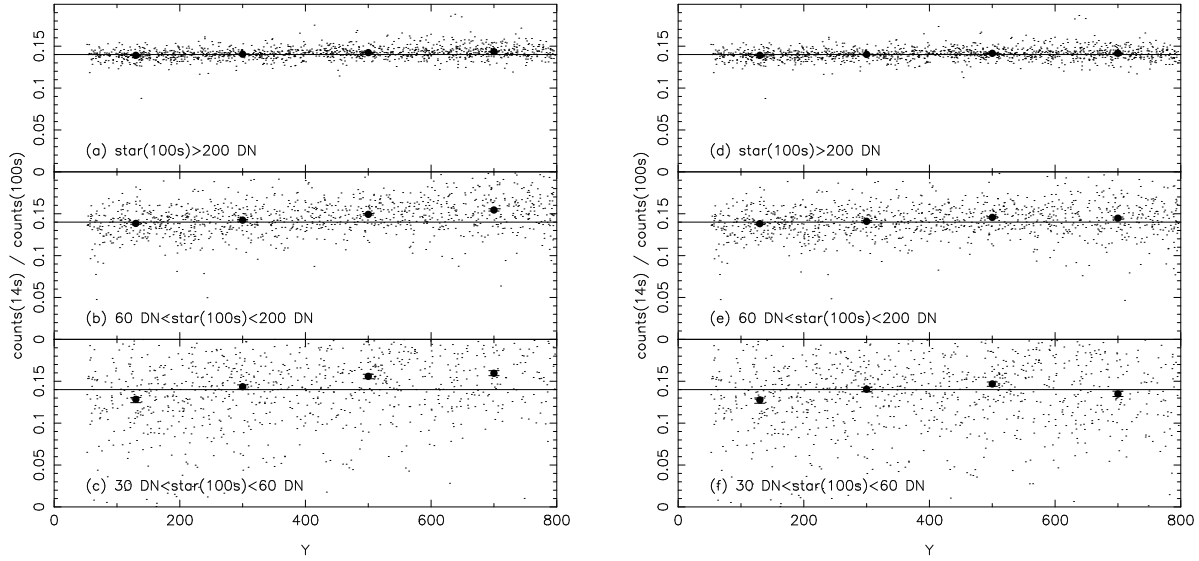


Fig. 6.— Ratio of counts from 14-second exposures to 100-second exposures, after applying CTE correction. The form of the CTE correction used in panels a-c fails to account for the change in CTE loss during readout, while that used in panels d-f account for this effect. The horizontal line is at 0.14, the expected ratio. The brightest stars (panels a and d) correspond to brightness levels of the calibration data used in this study (400 electrons and brighter in the short exposures). Note that CTE loss is overcorrected for the faintest stars when not accounting for CTE loss rate changes during readout.

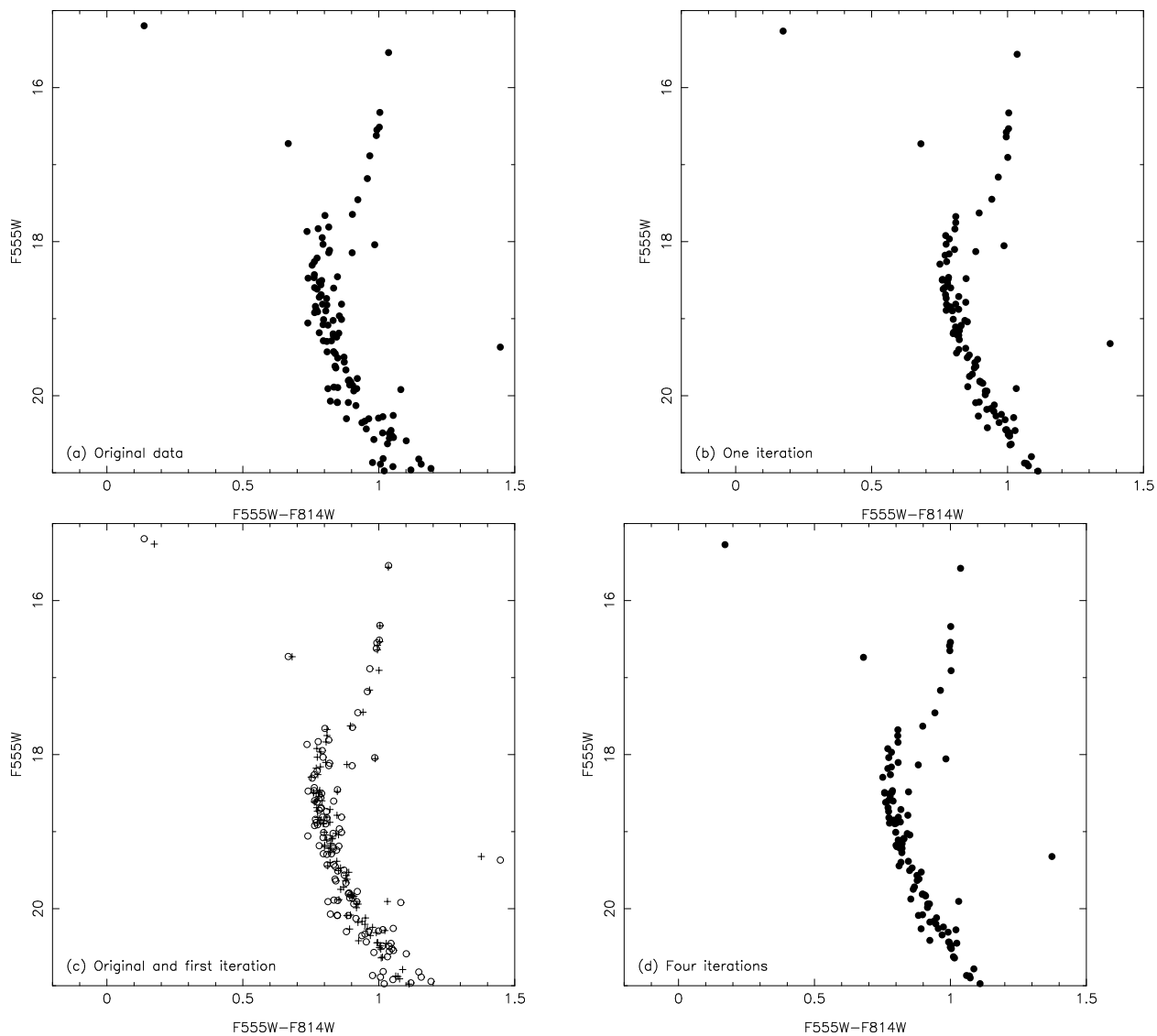


Fig. 7.— Standard photometry used in determining CTE corrections. Panel (a) shows the original photometry of Walker (1994), transformed into F555W and F814W instrumental magnitudes. Panel (b) shows the values obtained from CTE-corrected WFPC2 photometry, and panel (c) shows the first two panels overplotted. Note that the sequences lie overlaid, indicating that no significant photometry biases are introduced by using the WFPC2 data for a subsequent CTE solution. Finally, panel (d) shows the values from CTE-corrected WFPC2 photometry, after four iterations of re-computing standard magnitudes. The largest magnitude difference between this and panel (b) is 0.01.

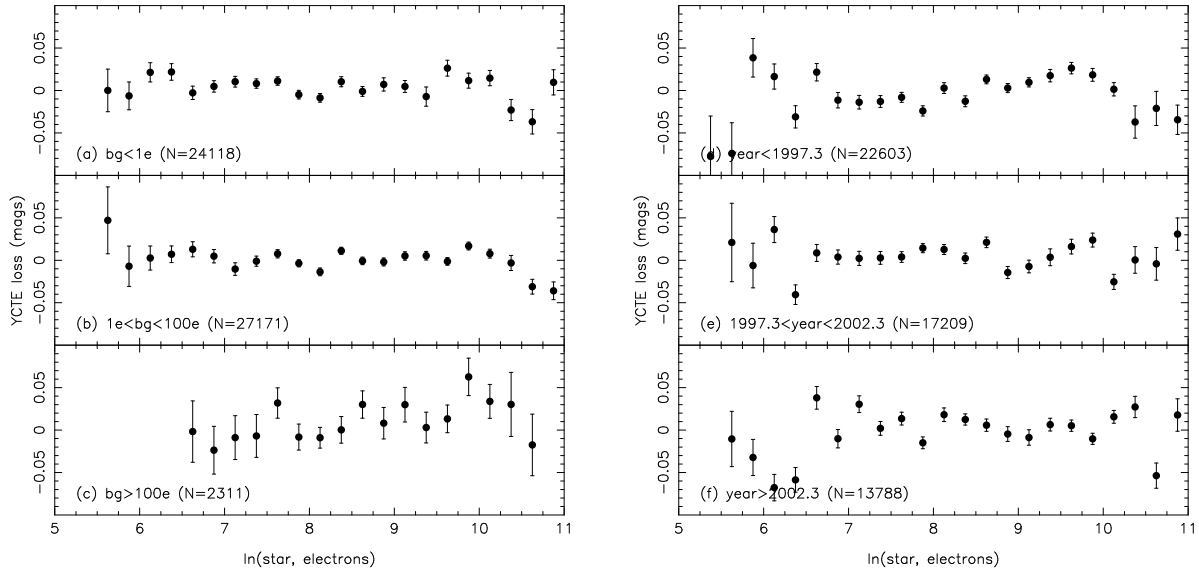


Fig. 8.— Residual YCTE losses (measured minus fit), as a function of star brightness. The left panels (a-c) show three different data samples selected by background level; the data in the right panels (d-f) are selected by observation date.

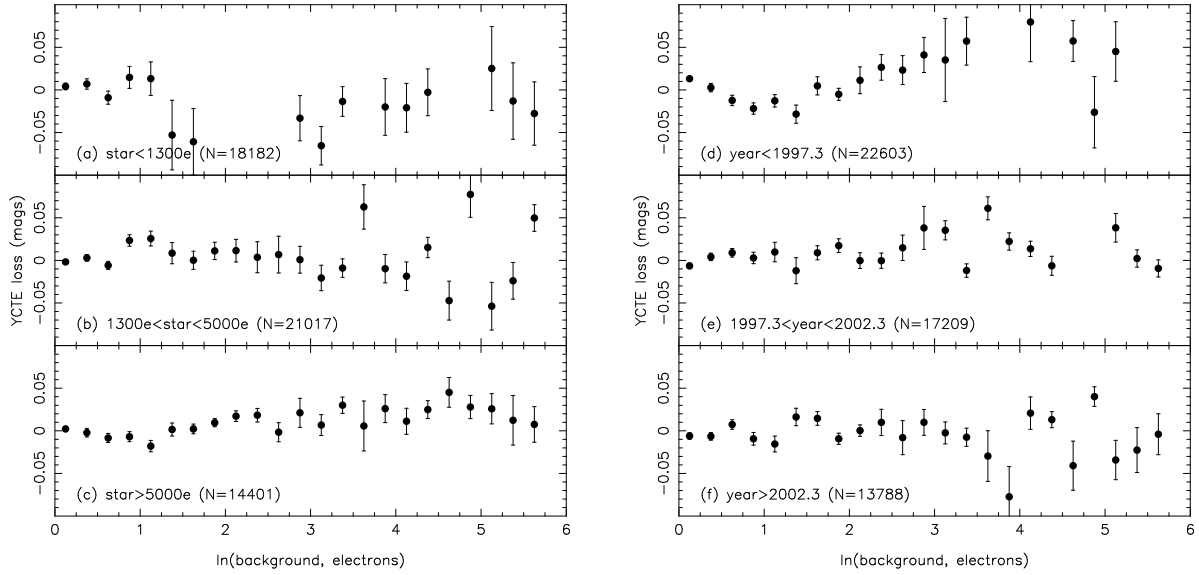


Fig. 9.— Residual YCTE losses (measured minus fit), as a function of background level. The left panels (a-c) show three different data samples selected by star brightness; the data in the right panels (d-f) are selected by observation date.

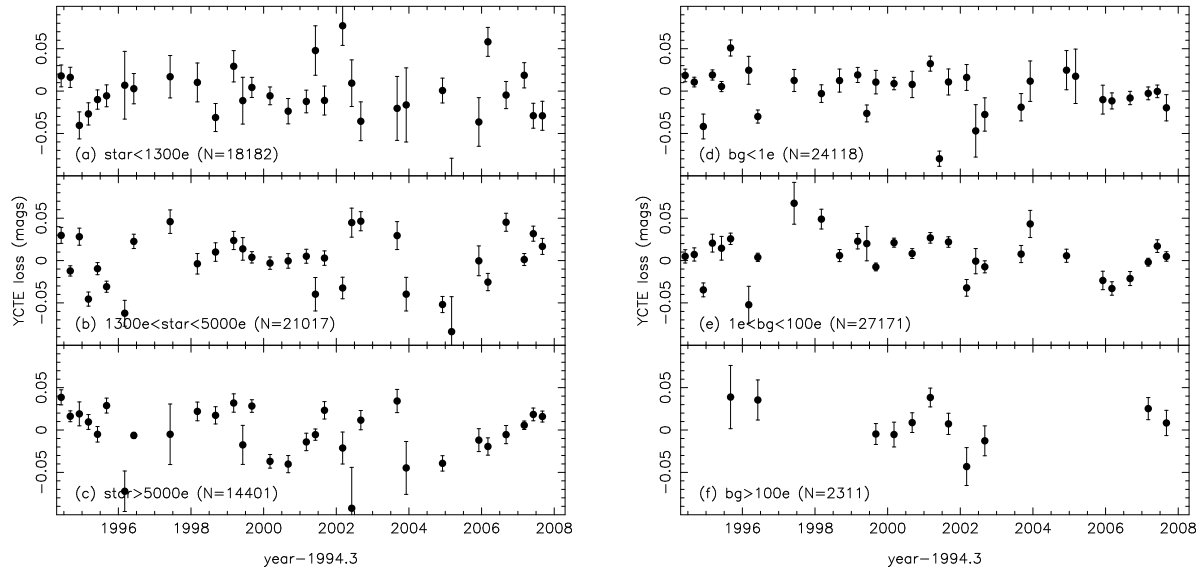


Fig. 10.— Residual YCTE losses (measured minus fit), as a function of observation date. The left panels (a-c) show three different data samples selected by star brightness; the data in the right panels (d-f) are selected by background level.

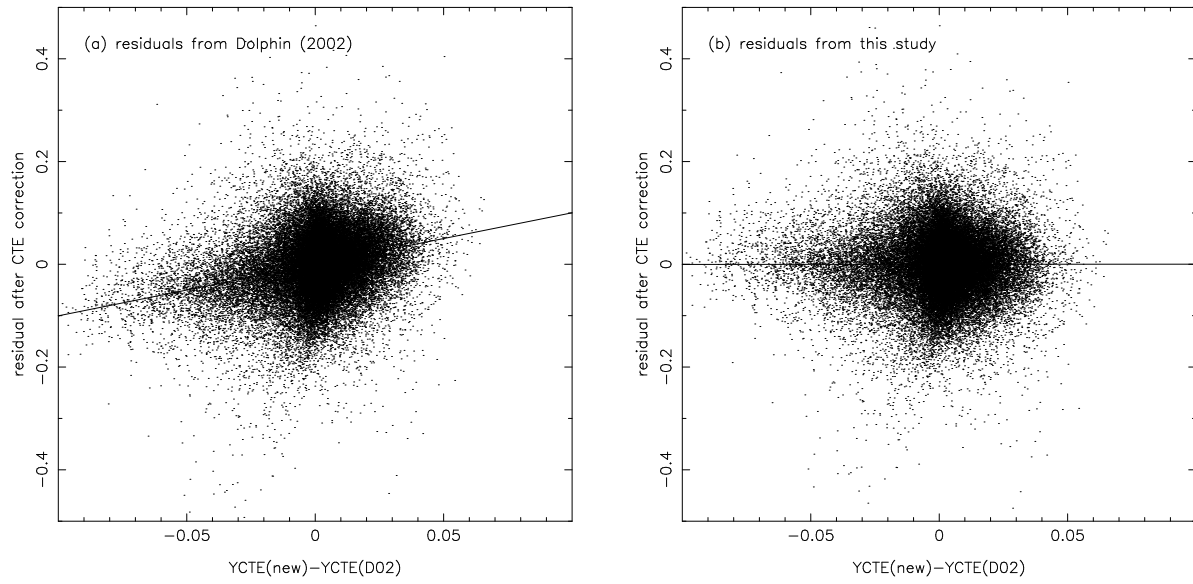


Fig. 11.— A comparison of the D02 CTE corrections with those from this study. Residuals after applying the D02 CTE correction (left panel) and the CTE correction from this study (right panel) are plotted against difference between the two corrections. The lines in each panel show the best fit to the data.

Table 1. Simple Statistics of Stellar Measurements Used for Calibration

Value	Brightness ^a	Background ^a	Epoch
minimum	106	0	29 April 1994
16%	666	0.16	25 December 1994
median	2226	1.16	15 June 1999
84%	8658	9.2	24 November 2005
maximum	59971	2229	21 August 2007

^aValues given in electrons

Table 2. Zero Points for GAIN=7

Filter	PC	WFC2	WFC3	WFC4
F380W	21.000 ± 0.009	21.012 ± 0.005	21.012 ± 0.005	20.996 ± 0.005
F410M	19.360 ± 0.009	19.373 ± 0.006	19.373 ± 0.005	19.356 ± 0.005
F439W	20.874 ± 0.008	20.886 ± 0.004	20.886 ± 0.004	20.870 ± 0.004
F450W	21.970 ± 0.009	21.982 ± 0.005	21.982 ± 0.005	21.966 ± 0.005
F467M	19.895 ± 0.009	19.908 ± 0.006	19.908 ± 0.005	19.891 ± 0.005
F547M	21.618 ± 0.003	21.627 ± 0.002	21.630 ± 0.003	21.609 ± 0.002
F555W	22.508 ± 0.003	22.517 ± 0.001	22.520 ± 0.002	22.499 ± 0.001
F569W	22.181 ± 0.003	22.190 ± 0.002	22.193 ± 0.003	22.172 ± 0.002
F606W	22.850 ± 0.003	22.859 ± 0.002	22.862 ± 0.003	22.841 ± 0.002
F622W	22.329 ± 0.009	22.340 ± 0.006	22.338 ± 0.007	22.327 ± 0.006
F675W	22.033 ± 0.007	22.044 ± 0.004	22.042 ± 0.004	22.030 ± 0.003
F702W	22.432 ± 0.008	22.443 ± 0.004	22.442 ± 0.005	22.430 ± 0.004
F785LP	20.635 ± 0.003	20.668 ± 0.003	20.670 ± 0.003	20.642 ± 0.003
F791W	21.441 ± 0.004	21.473 ± 0.004	21.475 ± 0.004	21.447 ± 0.004
F814W	21.591 ± 0.002	21.624 ± 0.001	21.625 ± 0.001	21.598 ± 0.001
F850LP	19.899 ± 0.005	19.932 ± 0.005	19.934 ± 0.005	19.906 ± 0.005
F1042M	16.189 ± 0.010	16.222 ± 0.010	16.224 ± 0.010	16.196 ± 0.010

Table 3. Zero Points for GAIN=14

Filter	PC	WFC2	WFC3	WFC4
F380W	20.234 ± 0.004	20.255 ± 0.003	20.237 ± 0.003	20.258 ± 0.003
F410M	18.595 ± 0.004	18.616 ± 0.004	18.598 ± 0.004	18.618 ± 0.004
F439W	20.108 ± 0.002	20.129 ± 0.001	20.111 ± 0.001	20.132 ± 0.002
F450W	21.204 ± 0.004	21.225 ± 0.003	21.207 ± 0.003	21.228 ± 0.004
F467M	19.130 ± 0.004	19.151 ± 0.004	19.133 ± 0.004	19.153 ± 0.004
F547M	20.867 ± 0.003	20.863 ± 0.002	20.871 ± 0.002	20.884 ± 0.002
F555W	21.757 ± 0.002	21.753 ± 0.001	21.761 ± 0.001	21.774 ± 0.002
F569W	21.430 ± 0.003	21.426 ± 0.002	21.434 ± 0.002	21.447 ± 0.003
F606W	22.099 ± 0.003	22.095 ± 0.002	22.103 ± 0.002	22.116 ± 0.002
F622W	21.564 ± 0.006	21.579 ± 0.005	21.576 ± 0.005	21.576 ± 0.006
F675W	21.268 ± 0.002	21.282 ± 0.001	21.280 ± 0.001	21.279 ± 0.003
F702W	21.667 ± 0.004	21.682 ± 0.003	21.679 ± 0.003	21.679 ± 0.004
F785LP	19.902 ± 0.003	19.915 ± 0.003	19.908 ± 0.003	19.912 ± 0.003
F791W	20.707 ± 0.004	20.720 ± 0.004	20.713 ± 0.004	20.717 ± 0.004
F814W	20.857 ± 0.001	20.870 ± 0.001	20.863 ± 0.001	20.867 ± 0.001
F850LP	19.166 ± 0.005	19.179 ± 0.005	19.172 ± 0.005	19.176 ± 0.005
F1042M	15.456 ± 0.010	15.468 ± 0.010	15.462 ± 0.010	15.466 ± 0.010

Table 4. *BVRI* Transformations

Filter	SMAG	SCOL	T1	T2	GAIN=7 Zero Points				GAIN=14 Zero Points				Cmin	Cmax
					PC	WFC2	WFC3	WFC4	PC	WFC2	WFC3	WFC4		
F380W	B	(B-V)	-0.581	0.777	21.025	21.037	21.037	21.021	20.259	20.280	20.262	20.283		0.5
F380W	B	(B-V)	-0.943	0.103	21.377	21.389	21.389	21.373	20.611	20.632	20.614	20.635	0.5	
F410M	B	(B-V)	-0.183	-0.287	19.670	19.683	19.683	19.666	18.905	18.926	18.908	18.928		
F439W	B	(U-B)	-0.103	-0.046	20.861	20.873	20.873	20.857	20.095	20.116	20.098	20.119		
F439W	B	(B-V)	0.003	-0.088	20.874	20.886	20.886	20.870	20.108	20.129	20.111	20.132		
F439W	B	(B-R)	0.019	-0.049	20.868	20.880	20.880	20.864	20.102	20.123	20.105	20.126		
F439W	B	(B-I)	0.005	-0.023	20.871	20.883	20.883	20.867	20.105	20.126	20.108	20.129		
F450W	B	(B-V)	0.230	-0.003	21.972	21.984	21.984	21.968	21.206	21.227	21.209	21.230		
F467M	B	(B-V)	0.480	-0.299	19.902	19.915	19.915	19.898	19.137	19.158	19.140	19.160		0.5
F467M	B	(B-V)	0.432	-0.002	19.853	19.866	19.866	19.849	19.088	19.109	19.091	19.111	0.5	
F547M	V	(B-V)	0.031	-0.039	21.613	21.622	21.625	21.604	20.862	20.858	20.866	20.879		1.0
F547M	V	(B-V)	0.056	-0.016	21.565	21.574	21.577	21.556	20.814	20.810	20.818	20.831	1.0	
F547M	V	(V-I)	0.027	-0.032	21.613	21.622	21.625	21.604	20.862	20.858	20.866	20.879		1.1
F547M	V	(V-I)	0.049	-0.013	21.565	21.574	21.577	21.556	20.814	20.810	20.818	20.831	1.1	
F555W	V	(U-V)	-0.014	0.005	22.489	22.498	22.501	22.480	21.738	21.734	21.742	21.755		
F555W	V	(B-V)	-0.060	0.033	22.508	22.517	22.520	22.499	21.757	21.753	21.761	21.774		
F555W	V	(V-R)	-0.121	0.120	22.513	22.522	22.525	22.504	21.762	21.758	21.766	21.779		
F555W	V	(V-I)	-0.052	0.027	22.508	22.517	22.520	22.499	21.757	21.753	21.761	21.774		
F569W	V	(V-I)	0.089	-0.003	22.179	22.188	22.191	22.170	21.428	21.424	21.432	21.445		2.0
F569W	V	(V-I)	-0.125	0.022	22.511	22.520	22.523	22.502	21.760	21.756	21.764	21.777	2.0	
F606W	V	(B-V)	0.293	0.015	22.859	22.868	22.871	22.850	22.108	22.104	22.112	22.125		1.7
F606W	V	(B-V)	-0.284	0.081	23.649	23.658	23.661	23.640	22.898	22.894	22.902	22.915	1.7	
F606W	V	(V-I)	0.254	0.012	22.859	22.868	22.871	22.850	22.108	22.104	22.112	22.125		2.0
F606W	V	(V-I)	-0.247	0.065	23.649	23.658	23.661	23.640	22.898	22.894	22.902	22.915	2.0	
F622W	R	(V-R)	-0.252	-0.111	22.343	22.354	22.352	22.341	21.578	21.593	21.590	21.590		
F675W	R	(U-R)	0.039	-0.007	22.053	22.064	22.062	22.050	21.288	21.302	21.300	21.299		
F675W	R	(B-R)	0.092	-0.017	22.034	22.045	22.043	22.031	21.269	21.283	21.281	21.280		
F675W	R	(V-R)	0.253	-0.125	22.033	22.044	22.042	22.030	21.268	21.282	21.280	21.279		
F675W	R	(R-I)	0.273	-0.066	22.024	22.035	22.033	22.021	21.259	21.273	21.271	21.270		
F702W	R	(V-R)	0.343	-0.177	22.437	22.448	22.447	22.435	21.672	21.687	21.684	21.684		0.6
F702W	R	(V-R)	0.486	-0.079	22.315	22.326	22.325	22.313	21.550	21.565	21.562	21.562	0.6	
F785LP	I	(V-I)	0.091	0.020	20.638	20.671	20.673	20.645	19.905	19.918	19.911	19.915		
F791W	I	(V-I)	-0.029	-0.004	21.441	21.473	21.475	21.447	20.707	20.720	20.713	20.717		1.0
F791W	I	(V-I)	-0.084	0.011	21.482	21.514	21.516	21.488	20.748	20.761	20.754	20.758	1.0	

Table 4—Continued

Filter	SMAG	SCOL	T1	T2	PC	GAIN=7 Zero Points			PC	GAIN=14 Zero Points			Cmin	Cmax
						WFC2	WFC3	WFC4		WFC2	WFC3	WFC4		
F814W	I	(U-I)	-0.018	0.002	21.567	21.600	21.601	21.574	20.833	20.846	20.839	20.843		
F814W	I	(B-I)	-0.031	0.007	21.587	21.620	21.621	21.594	20.853	20.866	20.859	20.863		
F814W	I	(V-I)	-0.062	0.025	21.591	21.624	21.625	21.598	20.857	20.870	20.863	20.867		
F814W	I	(R-I)	-0.112	0.084	21.591	21.624	21.625	21.598	20.857	20.870	20.863	20.867		
F850LP	I	(V-I)	0.160	0.023	19.881	19.914	19.916	19.888	19.148	19.161	19.154	19.158		
F1042M	I	(V-I)	0.350	0.022	16.136	16.169	16.171	16.143	15.403	15.415	15.409	15.413		